THE JOURNAL OF PHYSICAL CHEMISTRY C
A JOURNAL OF THE AMERICAN CHEMICAL SOCIETY

pubs.acs.org/JPCC

Article

Cobalt–Copper Nanoparticles on Three-Dimensional Substrate for Efficient Ammonia Synthesis via Electrocatalytic Nitrate Reduction

Published as part of The Journal of Physical Chemistry virtual special issue "Cynthia Friend Festschrift".

Tae Hwa Jeon, Zhen-Yu Wu, Feng-Yang Chen, Wonyong Choi,* Pedro J. J. Alvarez,* and Haotian Wang*

Cite This: *J. Phys. Chem. C* 2022, 126, 6982–6989

Read Online

ACCESS | Metrics & More | Article Recommendations | Supporting Information

ABSTRACT: Ammonia (NH_3) is a valuable chemical for fertilizer production and for use as an effective hydrogen carrier. Electrocatalytic nitrate reduction has recently received great attention as an alternative for NH_3 synthesis due to its kinetically favorable reaction. However, this promising strategy suffers from low Faradaic efficiency (FE) at large current density (>100 mA cm^{-2}) and low nitrate concentrations because of the competing hydrogen evolution reaction. Herein, we report a catalyst consisting of earth-abundant cobalt–copper ($Co_{1-x}Cu_x$) nanoparticles supported on a three-dimensional substrate for efficient and selective NH_3 synthesis via electrocatalytic nitrate reduction. Typically, the optimized $Co_{0.5}Cu_{0.5}$ catalyst performs at a high NH_3 Faradaic efficiency (FE) of over 95% at −0.03 V with NH_3 partial current density of ∼176 mA cm^{-2} at 50 mM nitrate, which is 7.3- and 1.7-fold higher than that of pure Co and Cu counterparts. Importantly, replacing Co with Cu enables the tuning of onset potential on Co catalyst maintaining high selectivity toward NH_3. A stability test over 12 cycles confirmed the long-term operation of this catalyst. This work offers a facile strategy for tuning the catalyst's elemental composition to attain a desired electrocatalytic activity.

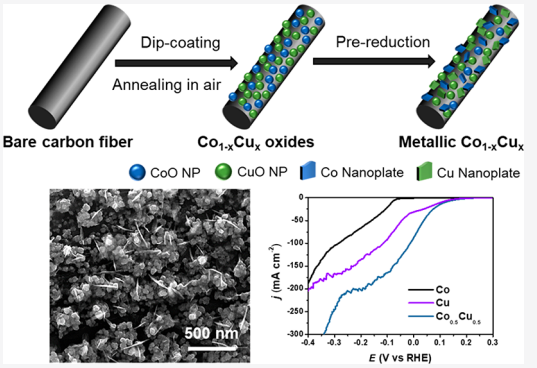

INTRODUCTION

Ammonia (NH_3) is a valuable chemical that is widely used as a building block in the manufacture of fertilizers.[1,2] It is also considered as a promising hydrogen energy carrier due to its higher hydrogen storage density (17.7 wt % in gravimetric and 121 kg m^{-3} in volumetric at 10 bar).[3] The industrial-scale production of NH_3 through the Haber–Bosch process is based on centralized large-scale production plants that use high temperature (400–650 °C) and pressure (200–400 atm) and emit massive amounts of carbon dioxide (typically, ∼1.8 t of CO_2 per t of NH_3 synthesis).[2−4] As an alternative, electrocatalytic nitrogen gas reduction (NRR) has been proposed for the green production of NH_3.[5−10] However, high NH_3 yield rates and Faradaic efficiencies (FE) have been elusive because the activation barrier of the N≡N bond dissociation is very high (945 kJ mol^{-1} for N≡N bond dissociation).[11,12] To date, only limited progress has been made to overcome this challenge, and the highest reported performance resulted in an NH_3 yield of 53 nmol s^{-1} cm^{-2} yield with an FE of ∼69%, which was achieved by using Li-mediated NRR with phosphonium cation as a proton shuttle.[13]

Electrocatalytic nitrate reduction (NO_3RR) has recently received extensive attention as a sustainable alternative for decentralized production of NH_3 with a high yield rate and FE.[14,15] The synthesis of NH_3 via nitrate (NO_3^-) reduction is thermodynamically more favorable compared to that via NRR (204 kJ mol^{-1} for N=O dissociation).[16] One reason NO_3RR is more attractive than NRR is that wastewater containing high nitrate concentrations can be used as a feedstock to obtain a versatile fuel (NH_3).[17−20] Selective conversion of NO_3^- to NH_3 in an alkaline medium proceeds through eight-electron transfer (eq 1):[21]

$$NO_3^- + 9H_2O + 8e^- \rightarrow NH_3 + 3H_2O + 9OH^- \quad (1)$$

Because NO_3^- could be transformed to other inorganic nitrogen species such as nitrite (NO_2^-), nitrogen monoxide (NO), nitrous oxide (N_2O), hydroxylamine (NH_2OH), and dinitrogen (N_2) as intermediate or final products,[22,23] there is growing interest in the rational designing of catalysts (including alloys,[24,25] single-atom catalysts,[26] molecular catalysts,[27] nanoclusters,[28] metal oxide,[29−31] and metal

Received: December 22, 2021
Revised: March 11, 2022
Published: April 19, 2022

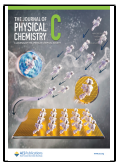

electrode[32,33]) that achieve selective NO_3RR to NH_3. In most cases, the critical challenge is the suppression of the competing hydrogen evolution reaction (HER), especially at high current density (>100 mA cm^{-2}) under low concentrations of nitrate (i.e., <100 mM), which consumes electrons otherwise available for NO_3^- reduction.[14] Hydrogen adsorption via water dissociation (i.e., initial step of HER; Volmer step) is also important to provide protons for hydrogenation of NO_3RR intermediates. Accordingly, robust HER with fast water dissociation kinetics should be avoided to achieve high selectivity and high FE for NH_3 production at high current density (>100 mA cm^{-2}) under low concentrations of nitrate.

Here we report an efficient and highly selective NO_3RR to NH_3 process in alkaline solution, catalyzed by earth-abundant cobalt−copper ($Co_{1-x}Cu_x$) nanoparticles on three-dimensional carbon fiber paper substrate. Both Co and Cu atoms are found to be present in metallic phase and interact synergistically to enhance NO_3RR performance. Replacing Co with Cu enhanced the current density and the Faradaic efficiency (FE) for NH_3, while the FE reached over 95% at $Co_{0.5}Cu_{0.5}$ catalyst. This is enabled by the positive shift of onset potential where HER can be minimized.

METHODS

Synthesis of $Co_{1-x}Cu_x$ Catalysts. $Co_{1-x}Cu_x$ nanoparticles are deposited on three-dimensional substrate via dip-coating and annealing processes.[34] The precursor solution for dip-coating was prepared as follow: 40 wt % of metal precursor ($Co(NO_3)_2{\cdot}6H_2O$ + $Cu(NO_3)_2{\cdot}2.5H_2O$) was dissolved in dimethylformamide (DMF) solvent. For different Co:Cu ratios, amounts of $Co(NO_3)_2{\cdot}6H_2O$ and $Cu(NO_3)_2{\cdot}2.5H_2O$ varied for desired ratios. After dissolving, the solution was transferred to hot plate at 100 °C. Once transferred, 5 wt % polyvinylpyrrolidone (PVP) was added to the solution, and the mixture was stirred for 30 min. After cooling the mixture, a piece of carbon fiber paper was immersed into solution, followed by drying in oven for 10 min. A carbon fiber paper was then transferred to furnace and annealed at 300 °C for 2 h under air. The temperature reached to 300 °C in 20 min. As-annealed catalysts further underwent an electrochemical reduction (i.e., prereduction) process to convert oxides into metallic form. For a typical prereduction, −1.8 V vs SCE (without *iR* compensation) was applied to the catalysts for 10 min in 1 M KOH.

Characterization. Scanning electron microscopy (SEM) was performed by using an FEI Quanta 400 ESEM FEG. High-resolution transmission electron microscopy (HR-TEM) and electron energy loss spectroscopy (EELS) were performed by using a JEM-2100F with a Cs-corrected line at the National Institute for Nanomaterials Technology (Pohang, Korea). X-ray photoelectron spectroscopy (XPS) was performed by using a Theta Probe AR-XPS System with monochromated Al Kα radiation as an X-ray source (1486.6 eV) at Korea Basic Science Institute (Busan Center, Korea). X-ray diffraction (XRD) was performed by using Rigaku SmartLab with Cu Kα radiation.

Electrocatalytic Nitrate Reduction. Electrocatalytic nitrate reduction was performed in a three-electrode system by using a BioLogic VMP3 workstation with a customized H-cell divided by Nafion membrane (Fuel Cell Store) containing 1 M KOH + 50 mM KNO_3 (pH = 14) electrolyte. Each part has a total volume of 25 mL. A Ni foam and the standard calomel electrode (SCE, CH Instruments) were used as the counter and reference electrodes, respectively. Potentials were measured and referred against the SCE. Unless otherwise specified, the measured potential values were converted to the corresponding values vs RHE by using the following relationships: V vs RHE = V vs SCE + 0.241 + 0.059 × pH. A constant potential was applied for the potentiostatic tests for 10 min at a stirring rate of 600 rpm. Products including ammonia and nitrite were quantified after each of the electrolysis (see below for detailed quantification methods). For cycling test, a constant potential of −0.03 V was applied to $Co_{0.5}Cu_{0.5}$ catalyst for 10 min, and the solution was collected for products analysis. Another cycle of nitrate reduction test was performed on the same catalyst at the same condition by refreshing the electrolyte. For long-term durability test, a constant potential of −0.03 V was applied to $Co_{0.5}Cu_{0.5}$ catalyst for 6 h. Aliquots (100 μL) of electrolyte were intermittently withdrawn from the working electrode solution with a syringe in each data point.

Quantification of Ammonia and Nitrite. The amounts of produced ammonia (NH_3) in the solution was quantified by using the modified indophenol blue method,[26,35,36] *which is one of the improved and faster characterization techniques for ammonia detection*. In brief, a 1 M NaOH solution containing 5 wt % salicylic acid + 5 wt % sodium citrate (denoted as solution A), 0.05 M NaClO (denoted as solution B), and 1.0 wt % $C_5FeN_6Na_2O$ (denoted as solution C) was prepared in advance. 2 mL of a solution diluted with DI water was mixed with 2 mL of solution A, 1 mL of solution B, and 0.2 mL of solution C. After 2 h of the reaction at room temperature, the absorbance was measured at 655 nm by using a UV−vis spectrophotometer (Shimadzu, UV-2600). Ammonium chloride (NH_4Cl) solutions were used for the standard calibration curves for ammonia (Figure S9).

The amounts of produced nitrite (NO_2^-) in the solution was quantified by using Griess Reagent.[26] In brief, a solution containing 0.2 g of *N*-(1-naphthyl)ethylenediamine dihydrochloride + 4 g of *p*-aminobenzenesulfonamide + 10 mL of phosphoric acid in 50 mL of DI water was prepared in advance. 5 mL of solution diluted with DI water was mixed with 0.1 mL of as-prepared solution. After 20 min of the reaction at room temperature, the absorbance was measured at 540 nm by using a UV−vis spectrophotometer. Potassium nitrite (KNO_2) solutions were used for the standard calibration curves for nitrite (Figure S9).

Calculation of Faradaic Efficiency and Energy Efficiency. The Faradaic efficiency (FE) of ammonia (NH_3) and nitrite (NO_2^-) conversion was calculated as follows:[26]

$$FE_{ammonia} = (8 \times F \times C_{ammonia} \times V/17 \times Q) \times 100\%$$

$$FE_{nitrite} = (2 \times F \times C_{nitrite} \times V/46 \times Q) \times 100\%$$

where F, $C_{ammonia}$, $C_{nitrite}$, V, and Q refer to the Faraday constant (96485 C mol^{-1}), measured NH_3 concentration, measured NO_2^- concentration, volume of the cathodic electrolyte, and the total charge passing the cell, respectively.

The half-cell energy efficiency (EE) of ammonia (NH_3) was calculated as follows:[3]

$$EE_{ammonia} = (1.23 - E^0) \times FE_{ammonia}/(1.23 - E)$$

where E^0, $FE_{ammonia}$, and E refer to the equilibrium potential of electrocatalytic nitrate reduction to ammonia (i.e., 0.69 V), Faradaic efficiency for ammonia, and applied potential (vs RHE with 100% *iR* correction). 1.23 V is the equilibrium

https://doi.org/10.1021/acs.jpcc.1c10781
J. Phys. Chem. C 2022, 126, 6982−6989

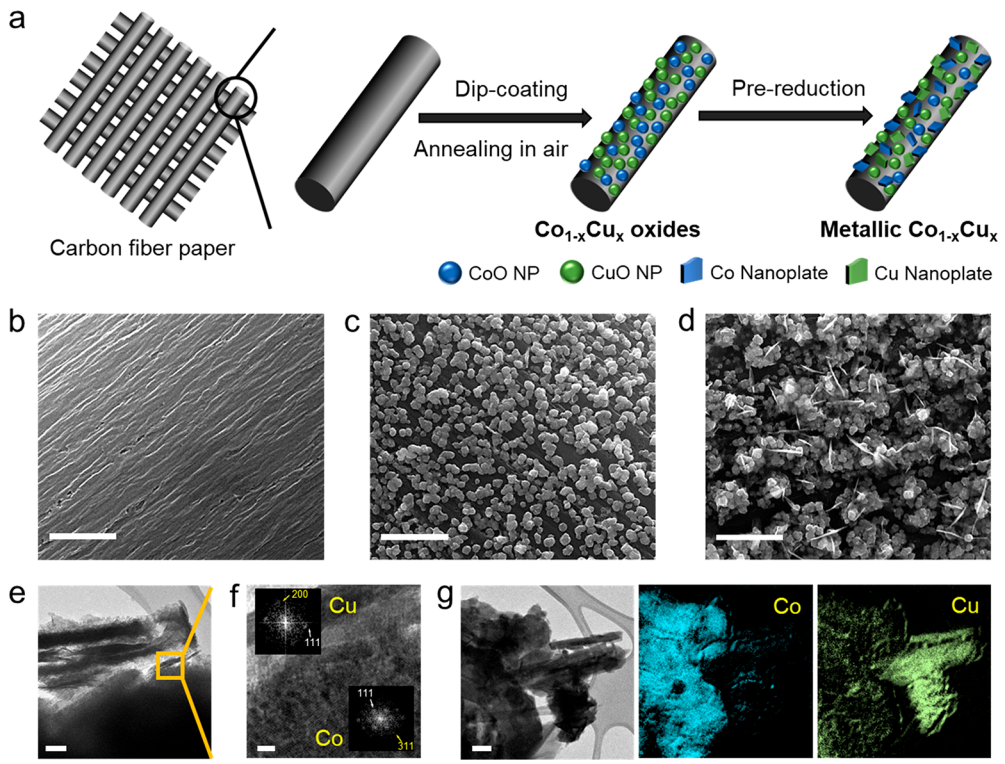

Figure 1. (a) Schematic illustration for the synthesis process of metallic cobalt−copper ($Co_{1-x}Cu_x$) catalysts on three-dimensional carbon fiber paper substrate. SEM images of (b) bare carbon paper, (c) $Co_{0.5}Cu_{0.5}$ oxides before prereduction, and (d) $Co_{0.5}Cu_{0.5}$ after prereduction. (e) HR-TEM and (f) enlarged images of $Co_{0.5}Cu_{0.5}$ from rectangular area in (e). FFT diffraction patterns in (f) represent the metallic cobalt and copper, respectively. (g) EELS mapping images of $Co_{0.5}Cu_{0.5}$. Scale bars are 500 nm in (b−d), 50 nm in (e), 4 nm in (f), and 100 nm in (g).

potential of water oxidation assuming zero overpotential of the water oxidation.

RESULTS AND DISCUSSION

Synthesis and Characterization of $Co_{1-x}Cu_x$ Catalysts. Cobalt−copper ($Co_{1-x}Cu_x$) nanoparticles on three-dimensional substrate was prepared via a dip-coating and annealing process (Figure 1a; see the Methods section for more details). A piece of carbon fiber paper was first immersed in as-prepared metal precursor−PVP solution with desired Co:Cu ratios, followed by annealing 300 °C for 2 h. The actual Co:Cu ratios of catalysts determined by ICP-OES analysis were similar to the ratios in precursor solution for dip-coating (Table S1). Scanning electron microscopy (SEM) images of as-annealed $Co_{0.5}Cu_{0.5}$ oxides catalyst exhibited small nanoparticle morphologies (Figure 1c; Figure S1 for other Co:Cu ratios), where PVP polymer prevented the particles from aggregation.[34]

As-annealed $Co_{0.5}Cu_{0.5}$ oxide catalyst was further electrochemically reduced, which induced a change in morphology (Figure 1d; Figure S2 for other Co:Cu ratios). Clearly, the nanoparticle morphologies did not result from the substrate (Figure 1b and Figure S3). Transmission electron microscopy (TEM) images of the catalysts before and after prereduction exhibited a clear change in morphologies from nanoparticles to nanoplates (Figures S4 and S5). High-resolution TEM (HR-TEM) and fast Fourier transform (FFT) diffraction patterns of $Co_{0.5}Cu_{0.5}$ catalyst after prereduction exhibited the coexistence of metallic cobalt and copper (Figure 1f). The lattice spacing of each particle further confirmed Cu (111) and Co (111) facets (Figure S6). Electron energy loss spectroscopy (EELS) mapping of $Co_{0.5}Cu_{0.5}$ catalyst also exhibited the individual structures of Co and Cu (Figure 1g).

The Co 2p XPS spectra of $Co_{0.5}Cu_{0.5}$ catalyst exhibited newly appeared peak at lower binding energy of main peak after prereduction, indicating the metallic Co (Figure 2a). However, the main peak contributed from cobalt oxides (CoO_x) is still present. This indicates that the Co phase was not fully reduced during prereduction. The Cu 2p XPS spectrum also indicates the change in oxidation states of Cu to metallic after prereduction, showing the notable main peak shifts to lower binding energy (Figure 2b). In addition, the satellite peaks of Cu 2p completely disappeared, which indicates that Cu was mainly present in metallic state. X-ray diffraction (XRD) patterns exhibited a clearer evidence of phases change from oxide to metallic form for the $Co_{0.5}Cu_{0.5}$ catalyst (Figure 2c,d). XRD patterns of pure Co and Cu catalysts before prereduction exhibited identical Co_3O_4 and CuO peaks, respectively (Figure 2e,f). However, these oxide forms of Co and Cu were not observed after prereduction. XRD patterns of all $Co_{1-x}Cu_x$ catalysts after prereduction exhibited metallic cobalt and copper peaks only (Figure 2c vs Figure S7). The intensities of metallic Co and Cu peaks varied for different Co:Cu ratios.

Electrocatalytic Nitrate Reduction of $Co_{1-x}Cu_x$ Catalysts. For the electrocatalytic NO_3RR performance of $Co_{1-x}Cu_x$ catalysts, a typical H-cell divided by Nafion membrane was used in 1 M KOH + 50 mM KNO_3 (pH = 14) electrolyte. The electrocatalytic activity of NO_3RR on $Co_{1-x}Cu_x$ catalysts was first investigated by using linear sweep voltammetry (Figure 3a and Figure S8). For $Co_{0.5}Cu_{0.5}$ catalyst, electrocatalytic hydrogen evolution reaction (HER) occurred from −0.2 V in the absence of nitrate in electrolyte

https://doi.org/10.1021/acs.jpcc.1c10781
J. Phys. Chem. C 2022, 126, 6982−6989

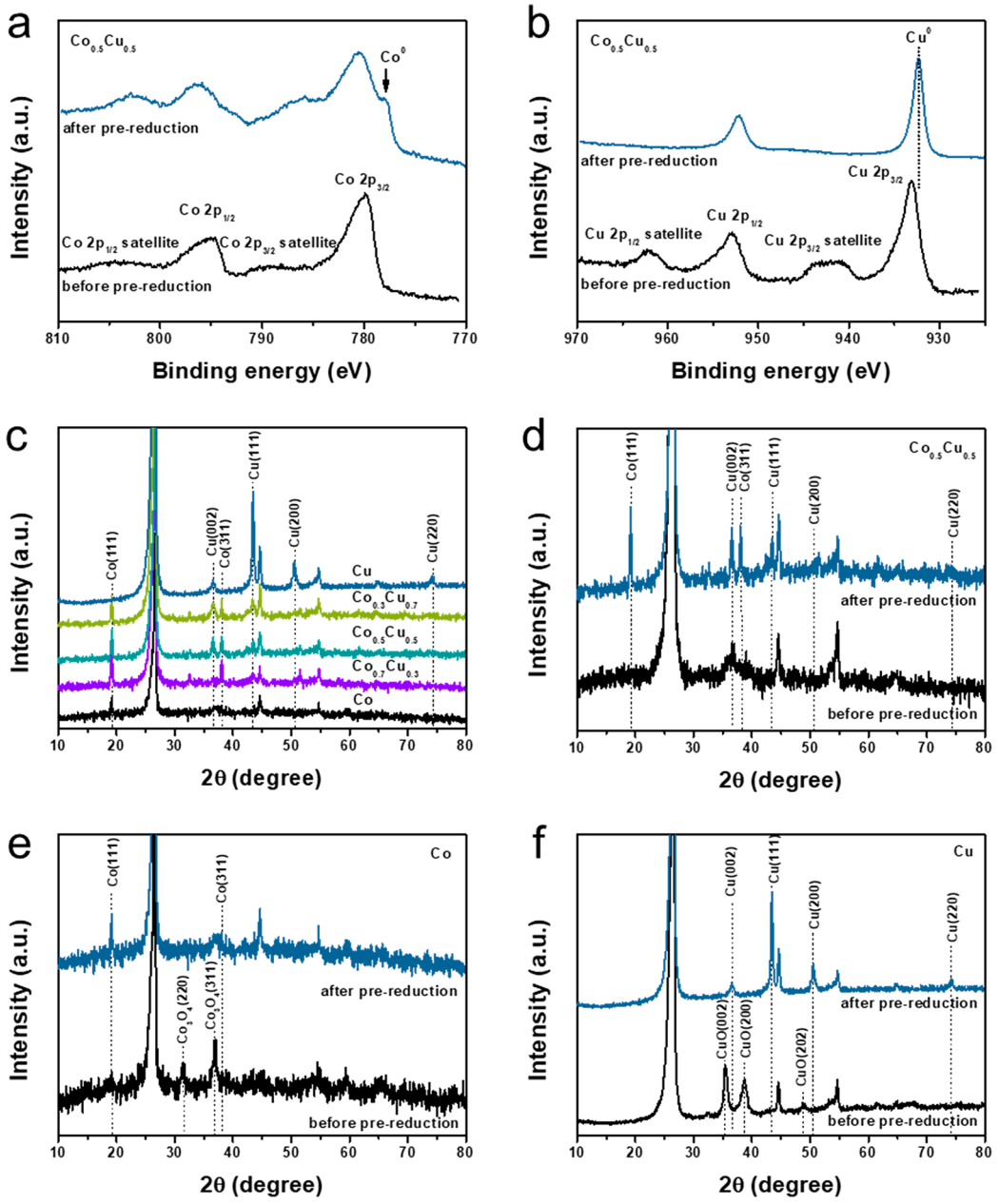

Figure 2. (a) Co 2p and (b) Cu 2p XPS spectra of $Co_{0.5}Cu_{0.5}$ before and after prereduction. (c) XRD patterns of catalysts with different Co:Cu ratios. Comparison of XRD patterns before and after prereduction for (d) $Co_{0.5}Cu_{0.5}$, (e) Co, and (f) Cu.

(Figure 3a). However, when nitrate was added to the electrolyte solution, an electrocatalytic NO_3RR current was generated at +0.1 V. The positive shift in reduction current generation reflects nitrate reduction activity by the $Co_{0.5}Cu_{0.5}$ catalyst. The positive shift of onset potential for NO_3RR was found for all $Co_{1-x}Cu_x$ catalysts compared to that of bare Co or Cu (Figure 3a and Figure S8). This indicates that $Co_{1-x}Cu_x$ catalysts can effectively reduce nitrate at more positive potentials, where HER can be completely suppressed.

The electrocatalytic activity of NO_3RR on each $Co_{1-x}Cu_x$ catalyst was further investigated by using $j-E$ plots (Figure 3b). The current in each point was evaluated by applying a constant potential. The $Co_{0.5}Cu_{0.5}$ catalyst exhibited the highest current density with a typical current density of ~177 mA cm^{-2} at −0.03 V. A pure Co catalyst requires more negative potential of −0.25 V to reach the similar current density for NO_3RR activity. By replacing Co with Cu, the $Co_{1-x}Cu_x$ catalysts exhibited a much lower NO_3RR onset potential. This indicates that Cu atoms enhance electrocatalytic NO_3RR activity. The enhanced NO_3RR activities by introducing Cu into Co is well-agreed with literatures, in which Cu acts as a promoter to improve initial reduction pathway of NO_3^- to NO_2^-.[37]

NH_3 selectivity was also investigated on each $Co_{1-x}Cu_x$ catalyst by measuring the NH_3 product concentrations at each potential (Figure 3c). Electrolysis was performed for 10 min in each potential (Figure S9). The NH_3 production was quantified colorimetrically by using ultraviolet−visible (UV−vis) spectrophotometry (Figure S10). $Co_{0.5}Cu_{0.5}$ catalyst exhibited the highest NH_3 selectivity with the maximal Faradaic efficiency (FE) of over 95% at −0.03 V. The electrocatalytic performances of different Co:Cu ratios indicate

https://doi.org/10.1021/acs.jpcc.1c10781
J. Phys. Chem. C 2022, 126, 6982−6989

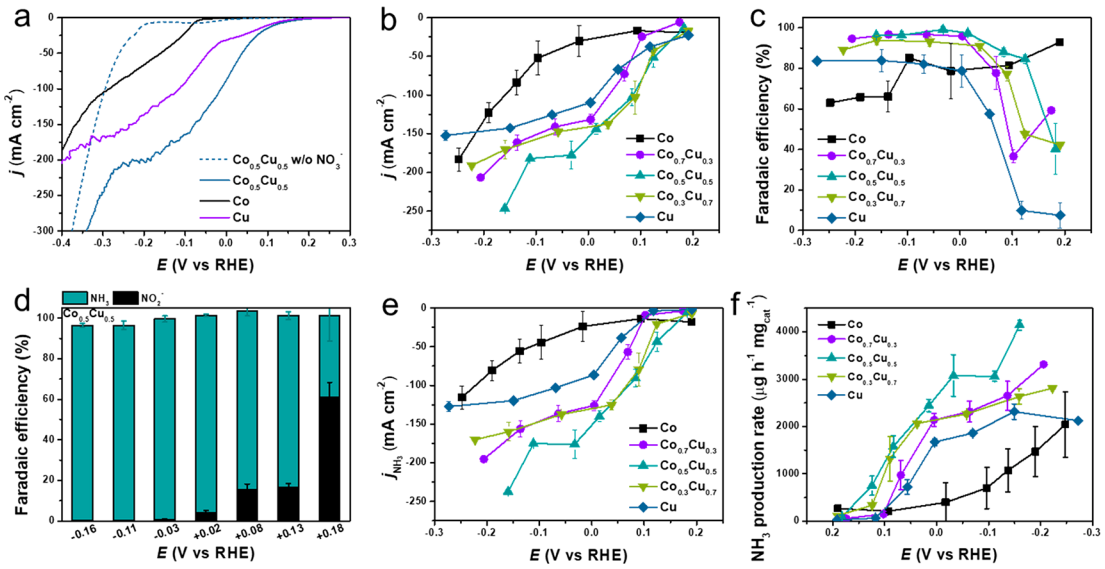

Figure 3. (a) Linear sweep voltammetry (70% *iR* corrected) of $Co_{0.5}Cu_{0.5}$, Co, and Cu in 1 M KOH electrolyte in the absence or presence of 0.05 M KNO_3. (b) *j*−*E* plots (100% *iR* corrected) and (c) NO_3^--to-NH_3 Faradaic efficiencies (FEs) of catalysts with different Co:Cu ratios in 1 M KOH + 0.05 M KNO_3 electrolyte. (d) NH_3 and NO_2^- FEs of $Co_{0.5}Cu_{0.5}$ with different potentials. (e) NH_3 partial current density (j_{NH_3}) of catalysts with different Co:Cu ratios. (f) NH_3 production rates for catalysts with different Co:Cu ratios. The error bars represent standard deviation from the mean of duplicate (or triplicate) electrolysis tests.

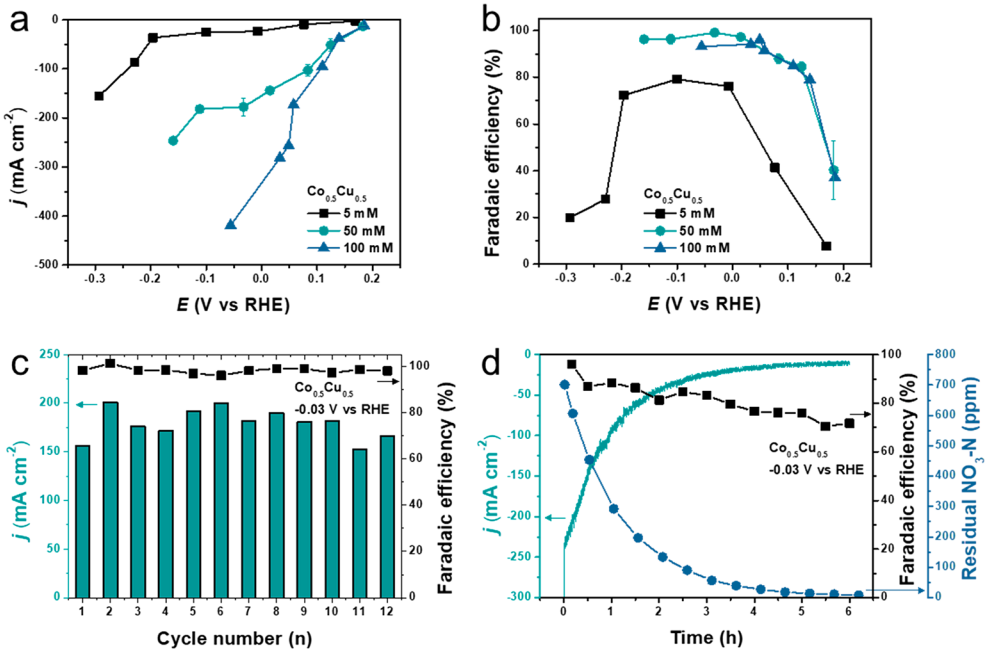

Figure 4. (a) *j*−*E* plots (100% *iR* corrected) and (b) NO_3^--to-NH_3 FEs of $Co_{0.5}Cu_{0.5}$ with different initial NO_3^- concentrations. The data of 50 mM (presented in Figure 3b,c) were included again for comparison. (c) Reuse tests of $Co_{0.5}Cu_{0.5}$ for NO_3^- reduction at −0.03 V. (d) Continuous electrochemical test of $Co_{0.5}Cu_{0.5}$ for NO_3^- reduction at −0.03 V.

the importance of composites formation between Co and Cu for NO_3RR. A pure Co catalyst exhibited high FE for NH_3 (80−90%) at positive potentials (lower current densities less than 25 mA cm^{-2}). This indicates that a pure Co catalyst has high NH_3 selectivity via NO_3RR. However, it competes with HER when a more negative potential is applied (<−0.1 V). Furthermore, a pure Cu catalyst exhibited higher current density at positive potential region than that of pure Co, indicating that Cu could reduce the overpotential of NO_3RR. Therefore, replacing Co with Cu could improve the catalytic activity of Co at a more positive potential while maintaining the high selectivity toward NH_3.

The presence of Co is also important since the NH_3 selectivity becomes much lower with the FE of <10% at >0.1 V in the absence of Co in the catalyst (i.e., pure Cu catalyst). In addition, the composites exhibited higher electrocatalytic performance and selectivity than pure catalysts. The products of NO_3RR on $Co_{0.5}Cu_{0.5}$ catalyst also exhibited more NO_2^- formation as the potential increased (Figure 3d). This indicates that introducing Cu atoms enhances the initial NO_3RR step

https://doi.org/10.1021/acs.jpcc.1c10781
J. Phys. Chem. C 2022, 126, 6982−6989

(NO_3^- + H_2O + $2e^-$ → NO_2^- + $2OH^-$). Because the NO_2^- formation is also considered as a rate-limiting step in NO_3RR to NH_3 (or N_2),[37] replacing Co with Cu could reduce the NO_3RR overpotential.

The NH_3 selectivity in NO_3RR on each $Co_{1-x}Cu_x$ catalyst was also compared in terms of NH_3 partial current density (j_{NH_3}), indicating that $Co_{0.5}Cu_{0.5}$ catalyst exhibited 7.3- and 1.7-fold increase in current density for NO_3RR to NH_3 at −0.03 V compared to that of pure Co and Cu, respectively (Figure 3e). The NH_3 production rates of $Co_{1-x}Cu_x$ catalysts were also determined with varying the composition (Figure 3f). Because the total (Co + Cu) amount loaded was similar (∼5 mg cm^{-2}) for all $Co_{1-x}Cu_x$ catalysts (Table S1), the differences in NO_3RR activity of $Co_{1-x}Cu_x$ are ascribed to the elemental composition.

The electrocatalytic NO_3RR activity and selectivity on $Co_{0.5}Cu_{0.5}$ catalyst was also investigated for different NO_3^- concentrations (Figure 4a,b). Electrolysis was also performed for 10 min in each potential (Figure S11). The current density increased as NO_3^- concentration increased, while the FE for NH_3 already reached its maximal values at 50 mM. At lower NO_3^- concentration (i.e., 5 mM), the catalyst promoted gas bubble evolution during the electrolysis, likely due to HER. However, no gas bubbles were observed during electrolysis at 50 or 100 mM NO_3^- over entire potential region.

To investigate the stability of $Co_{0.5}Cu_{0.5}$ catalyst regarding NH_3 selectivity, the cycling test of electrocatalytic NO_3RR was performed at −0.03 V (Figure 4c). The FE for NH_3 exhibited over 95% over 12 cycles of the electrolysis with the similar current density about 150−200 mA cm^{-2} in each cycle (Figure S12), indicating high stability of $Co_{0.5}Cu_{0.5}$ catalyst. The long-term durability of $Co_{0.5}Cu_{0.5}$ catalyst was also investigated. More than 95% of initial nitrate−nitrogen (NO_3−N) was removed from ∼700 to ∼7 ppm at −0.03 V over 6 h, and it was fully converted to NH_3 with a cumulative FE of ∼70% over 6 h. The decrease in current density over time is attributed to the decrease in NO_3^- concentration, indicating NO_3RR was responsible for the electrocatalytic activity. Considering that the U.S. Environmental Protection Agency (EPA) maximum contaminant Level (MCL) for NO_3−N in a public water supply is 10 mg/L,[38] the $Co_{0.5}Cu_{0.5}$ catalyst could meet the safe levels of nitrate over 6 h of electrolysis with a half-cell energy efficiency of ∼30%. This suggests that electrocatalytic treatment with $Co_{0.5}Cu_{0.5}$ could be a viable alternative for wastewater treatment with simultaneous recovery of a resource.

CONCLUSIONS

NH_3 can be synthesized with high yields and high FE via electrocatalytic NO_3RR mediated by $Co_{1-x}Cu_x$ nanoparticles deposited on a three-dimensional carbon fiber paper substrate. Co catalyst replaced with Cu by 50% ($Co_{0.5}Cu_{0.5}$) exhibited a highly improved NO_3RR activity and NH_3 selectivity, with a maximum FE for NH_3 of over 95% and a NH_3 partial current density of ∼176 mA cm^{-2}; this is 7.3- and 1.7-fold higher than that of pure Co and Cu catalyst, respectively, at 50 mM nitrate. The addition of Cu atoms decreases the overpotential in NO_3RR to increase the NH_3 FE at lower potential while inhibiting HER. Reuse cycles and continuous tests support the practical viability of this electrocatalytic system for the delocalized NH_3 synthesis and recovery from toxic nitrate anion in wastewaters.

ASSOCIATED CONTENT

Supporting Information

The Supporting Information is available free of charge at https://pubs.acs.org/doi/10.1021/acs.jpcc.1c10781.

Details about materials synthesis and characterization, experimental method, and data analysis; (Table S1 and Figures S1−S6) materials characterizations (SEM, HR-TEM, XPS, and XRD); (Figure S7) linear sweep voltammetric responses; (Figure S8, S10, S11) current transients; (Figure S9) quantitative detection of ammonia and nitrite (PDF)

AUTHOR INFORMATION

Corresponding Authors

Wonyong Choi − *KENTECH Institute for Environmental and Climate Technology, Korea Institute of Energy Technology (KENTECH), Naju 58330, Republic of Korea;* orcid.org/0000-0003-1801-9386; Email: wchoi@kentech.ac.kr

Pedro J. J. Alvarez − *Department of Chemical and Biomolecular Engineering and Department of Civil and Environmental Engineering, Rice University, Houston, Texas 77005, United States;* orcid.org/0000-0002-6725-7199; Email: alvarez@rice.edu

Haotian Wang − *Department of Chemical and Biomolecular Engineering, Department of Materials Science and NanoEngineering, and Department of Chemistry, Rice University, Houston, Texas 77005, United States;* orcid.org/0000-0002-3552-8978; Email: htwang@rice.edu

Authors

Tae Hwa Jeon − *Department of Chemical and Biomolecular Engineering and Department of Civil and Environmental Engineering, Rice University, Houston, Texas 77005, United States*

Zhen-Yu Wu − *Department of Chemical and Biomolecular Engineering, Rice University, Houston, Texas 77005, United States*

Feng-Yang Chen − *Department of Chemical and Biomolecular Engineering, Rice University, Houston, Texas 77005, United States;* orcid.org/0000-0002-3113-383X

Complete contact information is available at: https://pubs.acs.org/10.1021/acs.jpcc.1c10781

Author Contributions

T.H.J. and H.W. conceived the project. W.C., P.J.J.A., and H.W. supervised the project. T.H.J. designed the materials and performed the catalytic tests. T.H.J. performed the materials characterization. Z.-Y.W. and F.-Y.C. contributed to discussion on the data analysis. T.H.J., P.J.J.A, W.C., and H.W. wrote the manuscript. All authors participate in the discussion on the experimental results and commented on the manuscript.

Notes

The authors declare no competing financial interest.

ACKNOWLEDGMENTS

The authors acknowledge the support from Rice University, the National Science Foundation Nanosystems Engineering Research Center for Nanotechnology Enabled Water Treatment (NEWT EEC 1449500), and the Welch Foundation Research Grant (C-2051-20200401). The authors also

acknowledge the support from the Leading Researcher Program (NRF-2020R1A3B2079953) which was funded by the Korea government (MSIT) through the National Research Foundation of Korea (NRF). The authors thank Mr. Seungmok Han (POSTECH) for support with surface characterizations.

REFERENCES

(1) Tang, Y.; Mitchell, L. A.; Imler, G. H.; Parrish, D. A.; Shreeve, J. n. M. Ammonia Oxide as a Building Block for High-Performance and Insensitive Energetic Materials. *Angew. Chem., Int. Ed.* **2017**, *56* (21), 5894−5898.
(2) Erisman, J. W.; Sutton, M. A.; Galloway, J.; Klimont, Z.; Winiwarter, W. How a century of ammonia synthesis changed the world. *Nat. Geosci.* **2008**, *1* (10), 636−639.
(3) Andersson, J.; Grönkvist, S. Large-scale storage of hydrogen. *Int. J. Hydrogen Energy* **2019**, *44* (23), 11901−11919.
(4) Soloveichik, G. Electrochemical synthesis of ammonia as a potential alternative to the Haber−Bosch process. *Nat. Catal.* **2019**, *2* (5), 377−380.
(5) Guo, W.; Zhang, K.; Liang, Z.; Zou, R.; Xu, Q. Electrochemical nitrogen fixation and utilization: theories, advanced catalyst materials and system design. *Chem. Soc. Rev.* **2019**, *48* (24), 5658−5716.
(6) Foster, S. L.; Bakovic, S. I. P.; Duda, R. D.; Maheshwari, S.; Milton, R. D.; Minteer, S. D.; Janik, M. J.; Renner, J. N.; Greenlee, L. F. Catalysts for nitrogen reduction to ammonia. *Nat. Catal.* **2018**, *1* (7), 490−500.
(7) Qiu, W.; Xie, X.-Y.; Qiu, J.; Fang, W.-H.; Liang, R.; Ren, X.; Ji, X.; Cui, G.; Asiri, A. M.; Cui, G.; Tang, B.; Sun, X. High-performance artificial nitrogen fixation at ambient conditions using a metal-free electrocatalyst. *Nat. Commun.* **2018**, *9* (1), 3485.
(8) Lee, H. K.; Koh, C. S. L.; Lee, Y. H.; Liu, C.; Phang, I. Y.; Han, X.; Tsung, C.-K.; Ling, X. Y. Favoring the unfavored: selective electrochemical nitrogen fixation using a reticular chemistry approach. *Sci. Adv.* **2018**, *4* (3), eaar3208.
(9) Cheng, H.; Cui, P.; Wang, F.; Ding, L. X.; Wang, H. High efficiency electrochemical nitrogen fixation achieved with a lower pressure reaction system by changing the chemical equilibrium. *Angew. Chem., Int. Ed.* **2019**, *131* (43), 15687−15693.
(10) Fang, Z.; Wu, P.; Qian, Y.; Yu, G. Gel-Derived Amorphous Bismuth−Nickel Alloy Promotes Electrocatalytic Nitrogen Fixation via Optimizing Nitrogen Adsorption and Activation. *Angew. Chem., Int. Ed.* **2021**, *60* (8), 4275−4281.
(11) Gambarotta, S.; Scott, J. Multimetallic cooperative activation of N_2. *Angew. Chem., Int. Ed.* **2004**, *43* (40), 5298−5308.
(12) Ye, T.-N.; Park, S.-W.; Lu, Y.; Li, J.; Sasase, M.; Kitano, M.; Hosono, H. Contribution of Nitrogen Vacancies to Ammonia Synthesis over Metal Nitride Catalysts. *J. Am. Chem. Soc.* **2020**, *142* (33), 14374−14383.
(13) Suryanto, B. H.; Matuszek, K.; Choi, J.; Hodgetts, R. Y.; Du, H.-L.; Bakker, J. M.; Kang, C. S.; Cherepanov, P. V.; Simonov, A. N.; MacFarlane, D. R. Nitrogen reduction to ammonia at high efficiency and rates based on a phosphonium proton shuttle. *Science* **2021**, *372* (6547), 1187−1191.
(14) van Langevelde, P. H.; Katsounaros, I.; Koper, M. T. Electrocatalytic nitrate reduction for sustainable ammonia production. *Joule* **2021**, *5* (2), 290−294.
(15) Lu, X.; Song, H.; Cai, J.; Lu, S. Recent Development of Electrochemical Nitrate Reduction to Ammonia: A Mini Review. *Electrochem. Commun.* **2021**, *129*, 107094.
(16) Stirling, A.; Pápai, I.; Mink, J.; Salahub, D. R. Density functional study of nitrogen oxides. *J. Chem. Phys.* **1994**, *100* (4), 2910−2923.
(17) Fajardo, A. S.; Westerhoff, P.; Sanchez-Sanchez, C. M.; Garcia-Segura, S. Earth-abundant elements a sustainable solution for electrocatalytic reduction of nitrate. *Appl. Catal., B* **2021**, *281*, 119465.
(18) Garcia-Segura, S.; Lanzarini-Lopes, M.; Hristovski, K.; Westerhoff, P. Electrocatalytic reduction of nitrate: Fundamentals to full-scale water treatment applications. *Appl. Catal., B* **2018**, *236*, 546−568.
(19) Duca, M.; Koper, M. T. Powering denitrification: the perspectives of electrocatalytic nitrate reduction. *Energy Environ. Sci.* **2012**, *5* (12), 9726−9742.
(20) Su, L.; Han, D.; Zhu, G.; Xu, H.; Luo, W.; Wang, L.; Jiang, W.; Dong, A.; Yang, J. Tailoring the assembly of iron nanoparticles in carbon microspheres toward high-performance electrocatalytic denitrification. *Nano Lett.* **2019**, *19* (8), 5423−5430.
(21) Milazzo, G.; Caroli, S.; Braun, R. D. Tables of standard electrode potentials. *J. Electrochem. Soc.* **1978**, *125* (6), 261C.
(22) Katsounaros, I.; Dortsiou, M.; Polatides, C.; Preston, S.; Kypraios, T.; Kyriacou, G. Reaction pathways in the electrochemical reduction of nitrate on tin. *Electrochim. Acta* **2012**, *71*, 270−276.
(23) Wang, Y.; Wang, C.; Li, M.; Yu, Y.; Zhang, B. Nitrate electroreduction: mechanism insight, in situ characterization, performance evaluation, and challenges. *Chem. Soc. Rev.* **2021**, *50*, 6720.
(24) Wang, Y.; Xu, A.; Wang, Z.; Huang, L.; Li, J.; Li, F.; Wicks, J.; Luo, M.; Nam, D.-H.; Tan, C.-S.; et al. Enhanced nitrate-to-ammonia activity on copper−nickel alloys via tuning of intermediate adsorption. *J. Am. Chem. Soc.* **2020**, *142* (12), 5702−5708.
(25) Wang, Z.; Young, S. D.; Goldsmith, B. R.; Singh, N. Increasing electrocatalytic nitrate reduction activity by controlling adsorption through PtRu alloying. *J. Catal.* **2021**, *395*, 143−154.
(26) Wu, Z.-Y.; Karamad, M.; Yong, X.; Huang, Q.; Cullen, D. A.; Zhu, P.; Xia, C.; Xiao, Q.; Shakouri, M.; Chen, F.-Y.; et al. Electrochemical ammonia synthesis via nitrate reduction on Fe single atom catalyst. *Nat. Commun.* **2021**, *12* (1), 2870.
(27) Chen, G.-F.; Yuan, Y.; Jiang, H.; Ren, S.-Y.; Ding, L.-X.; Ma, L.; Wu, T.; Lu, J.; Wang, H. Electrochemical reduction of nitrate to ammonia via direct eight-electron transfer using a copper−molecular solid catalyst. *Nat. Energy* **2020**, *5* (8), 605−613.
(28) Li, J.; Zhan, G.; Yang, J.; Quan, F.; Mao, C.; Liu, Y.; Wang, B.; Lei, F.; Li, L.; Chan, A. W. Efficient ammonia electrosynthesis from nitrate on strained ruthenium nanoclusters. *J. Am. Chem. Soc.* **2020**, *142* (15), 7036−7046.
(29) Jia, R.; Wang, Y.; Wang, C.; Ling, Y.; Yu, Y.; Zhang, B. Boosting selective nitrate electroreduction to ammonium by constructing oxygen vacancies in TiO_2. *ACS Catal.* **2020**, *10* (6), 3533−3540.
(30) Wang, Y.; Zhou, W.; Jia, R.; Yu, Y.; Zhang, B. Unveiling the activity origin of a copper-based electrocatalyst for selective nitrate reduction to ammonia. *Angew. Chem., Int. Ed.* **2020**, *132* (13), 5388−5392.
(31) Daiyan, R.; Tran-Phu, T.; Kumar, P.; Iputera, K.; Tong, Z.; Leverett, J.; Khan, M. H. A.; Esmailpour, A. A.; Jalili, A.; Lim, M.; et al. Nitrate reduction to ammonium: from CuO defect engineering to waste NO_x-to-NH_3 economic feasibility. *Energy Environ. Sci.* **2021**, *14*, 3588.
(32) McEnaney, J. M.; Blair, S. J.; Nielander, A. C.; Schwalbe, J. A.; Koshy, D. M.; Cargnello, M.; Jaramillo, T. F. Electrolyte engineering for efficient electrochemical nitrate reduction to ammonia on a titanium electrode. *ACS Sustain. Chem. Eng.* **2020**, *8* (7), 2672−2681.
(33) Liu, H.; Park, J.; Chen, Y.; Qiu, Y.; Cheng, Y.; Srivastava, K.; Gu, S.; Shanks, B. H.; Roling, L. T.; Li, W. Electrocatalytic Nitrate Reduction on Oxide-Derived Silver with Tunable Selectivity to Nitrite and Ammonia. *ACS Catal.* **2021**, *11* (14), 8431−8442.
(34) Wang, H.; Lu, Z.; Kong, D.; Sun, J.; Hymel, T. M.; Cui, Y. Electrochemical tuning of MoS_2 nanoparticles on three-dimensional substrate for efficient hydrogen evolution. *ACS Nano* **2014**, *8* (5), 4940−4947.
(35) Zhao, Y.; Wu, F.; Miao, Y.; Zhou, C.; Xu, N.; Shi, R.; Wu, L. Z.; Tang, J.; Zhang, T. Revealing ammonia quantification minefield in photo/electrocatalysis. *Angew. Chem., Int. Ed.* **2021**, *133* (40), 21896−21899.
(36) Zhao, Y.; Shi, R.; Bian, X.; Zhou, C.; Zhao, Y.; Zhang, S.; Wu, F.; Waterhouse, G. I. N.; Wu, L.-Z.; Tung, C.-H.; Zhang, T. Ammonia detection methods in photocatalytic and electrocatalytic experiments:

https://doi.org/10.1021/acs.jpcc.1c10781
J. Phys. Chem. C 2022, 126, 6982−6989

how to improve the reliability of NH3 production rates? *Adv. Sci.* **2019**, *6* (8), 1802109.
(37) Chen, T.; Li, Y.; Li, L.; Zhao, Y.; Shi, S.; Jiang, R.; Ma, H. Cu Modified Pt Nanoflowers with Preferential (100) Surfaces for Selective Electroreduction of Nitrate. *Catalysts* **2019**, *9* (6), 536.
(38) Fan, A. M.; Steinberg, V. E. Health implications of nitrate and nitrite in drinking water: an update on methemoglobinemia occurrence and reproductive and developmental toxicity. *Regul. Toxicol. Pharmacol.* **1996**, *23* (1), 35−43.

https://doi.org/10.1021/acs.jpcc.1c10781
J. Phys. Chem. C 2022, 126, 6982−6989